Characterizing spinning black hole binaries in eccentric orbits with LISA

Joey Shapiro Key and Neil J. Cornish

Characterizing Spinning Black Hole Binaries in Eccentric Orbits with LISA

Joey Shapiro Key and Neil J. Cornish

Department of Physics, Montana State University, Bozeman, MT 59717

The Laser Interferometer Space Antenna (LISA) is designed to detect gravitational wave signals from astrophysical sources, including those from coalescing binary systems of compact objects such as black holes. Colliding galaxies have central black holes that sink to the center of the merged galaxy and begin to orbit one another and emit gravitational waves. Some galaxy evolution models predict that the binary black hole system will enter the LISA band with significant orbital eccentricity, while other models suggest that the orbits will already have circularized. Using a full seventeen parameter waveform model that includes the effects of orbital eccentricity, spin precession and higher harmonics, we investigate how well the source parameters can be inferred from simulated LISA data. Defining the reference eccentricity as the value one year before merger, we find that for typical LISA sources, it will be possible to measure the eccentricity to an accuracy of parts in a thousand. The accuracy with which the eccentricity can be measured depends only very weakly on the eccentricity, making it possible to distinguish circular orbits from those with very small eccentricities. LISA measurements of the orbital eccentricity can help constraints theories of galaxy mergers in the early universe. Failing to account for the eccentricity in the waveform modeling can lead to a loss of signal power and bias the estimation of parameters such as the black hole masses and spins.

I. INTRODUCTION

Binary systems of compact objects will be ubiquitous sources for the Laser Interferometer Space Antenna (LISA) [1, 2]. Observations have shown that today there are massive black holes in the center of nearly all galaxies [3–5]. When galaxies collide their central black holes sink to the center of the merged galaxy and begin to orbit one another, losing energy and angular momentum in the form of gravitational waves [6]. Gravitational wave (GW) emission rapidly erases any initial eccentricity [7, 8], so it has long been thought that eccentricity could be ignored when modeling the signals from massive black hole binaries [9]. More recently, however, it has been shown that the mechanisms that may harden the binary to the point where the gravitational wave emission takes over all tend to drive up the eccentricity [10–19]. The question then is whether significant eccentricity survives until the final year or so before merger. Figure 1 shows the eccentricity evolution as a function of orbital frequency for systems that enter the gravitational wave dominated evolution stage at frequency $f_{\rm gw}$ with eccentricities of $e_{\rm gw} = 0.95$ and $e_{\rm gw} = 0.5$. The tracks are computed using the leading-order Peters and Matthews [8] evolution equations. These equations predict that once the eccentricity drops below $e \sim 0.3$, it decays as $e \sim f^{-19/18}$ - in other words, roughly a factor of ten in eccentricity is lost per decade of frequency. The rate of decay is slower for systems with very high eccentricities, allowing them to maintain significant eccentricity for longer. For typical LISA black hole binaries, the GW decay time drops below the Hubble time when the systems are 3 to 5 decades in frequency from the LISA band, so unless $e_{\rm gw}$ is very close to unity, a purely GW driven orbital evolution results in nearly circular orbits in the LISA band. On the other hand, if the hardening mechanism (*e.g.* gas dynamics or stellar scattering) continues to dominate the

dynamics until the system is close to the LISA band, then interesting eccentricities can be maintained. In a
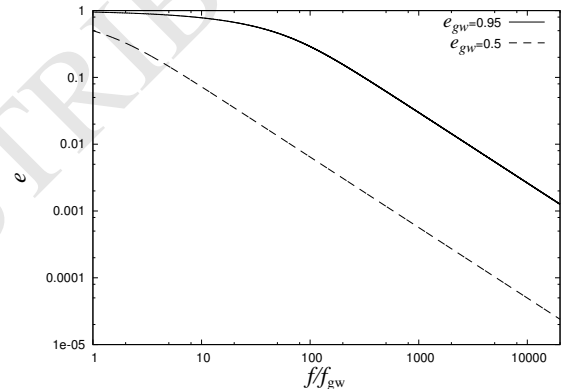

FIG. 1: Gravitational wave driven eccentricity evolution as a function of orbital frequency.

recent study [20], Sesana has shown that stellar scattering produces LISA sources with eccentricities in the range $e_0 = 10^{-3} \to 0.2$. Moreover, as shown in Figure 8 of Ref. [20], the distribution of eccentricities depends on the component masses in a particular way, so measuring this distribution can help constrain black hole merger models. While the distribution of component masses and spins as a function of luminosity distance will likely play a more important role in studying galaxy - black hole co-evolution [21–23], the eccentricity distribution may provide useful additional constraints. These considerations suggest that it is desirable to include the effects of eccentricity in the gravitational waveform, bringing the total number of parameters needed to describe a black hole inspiral to seventeen: the redshifted black hole masses (m_1, m_2), the distance to the source (D_L), the initial radial eccentricity and semi-major axis (e_0, a_0), the

dimensionless spin parameters for the two black holes (χ_1, χ_2), the source sky location $(\cos\theta, \phi)$, the initial orientation of the angular momentum and spin vectors $(\cos\theta_L, \phi_L), (\cos\theta_{S_1}, \phi_{S_1}), (\cos\theta_{S_2}, \phi_{S_2})$, and two initial phase parameters (n_0, ϕ_0). Failing to include the eccentricity in the waveform model will lead to a loss of signal-to-noise [24, 25] and to biases in the recovery of the other parameters [26, 27].

The instantaneous gravitational waveforms describing the inspiral of a black hole binary with arbitrary spins, masses, and orbital eccentricity were calculated by Kidder [28] to second post-Newtonian order ($2\,\mathrm{PN}$, or order v^4/c^4 in the relative velocity), and extended to $2.5\,\mathrm{PN}$ order by Faye, Blanchet and Buonanno [29, 30]. Majár and Vasúth [31] later introduced a convenient framework for expressing the waveforms in a form amenable to producing detection templates. Together with a solution to the conservative equations of motion, adiabatically advanced with the angular momentum and energy dissipation equations [28], we can build the time dependent gravitational waveforms for a general binary black hole system with the full seventeen parameters necessary to describe the system. LISA observations of binary black hole inspirals can be compared to these waveforms to produce posterior distributions for the model parameters. These observations will allow us to constrain galaxy merger scenarios [21–23], and allow us to test General Relativity in the dynamical strong field regime [32]. Left unaccounted for, the effects of orbital eccentricity may be mistaken for a departure from General Relativity (in particular, even small eccentricities that produce negligible power in higher harmonics can lead to easily detectable changes in the phase evolution of the signal).

Black hole binary systems in eccentric orbits may also be detected by ground based gravitational wave detectors such as the Laser Interferometer Gravitational wave Observatory (LIGO) and Virgo [33]. Some models even predict that inspiral signals may enter the LIGO band with $e > 0.9$ and that eccentric templates will be necessary to detect such sources [34]. Current LIGO data analysis uses circular templates and may need to be generalized to include eccentricity.

We have previously described a method for combining the instantaneous gravitational waveforms for eccentric binary systems with a post-Keplerian solution to the equations of motion that is adiabatically advanced using the the orbit-averaged dissipation and spin precession equations to build ready-to-use gravitational waveforms for the general case of a spinning black hole binary system in an eccentric orbit [35]. Here we present the results of a parameter estimation study for spinning eccentric binary black hole sources for the LISA mission. This is an extension of the Lang and Hughes LISA parameter estimation study of spinning binary black holes in circular orbits [36] and is the first to include the full seventeen parameters that describe a general black hole binary inspiral.

II. WAVEFORM MODEL

The equations needed to numerically calculate time dependent gravitational waveforms for binary black hole systems have been computed to 2.5PN order in the amplitude and phase [28–31]. The resulting system of equations could be numerically evolved to produce waveforms for our study, but the computational cost of resolving the motion of the black holes on the orbital timescale is too large for the parameter estimation study we wish to perform. Taking advantage of the separation of time scales in the waveform model we have developed an efficient waveform generator at 1.5 PN order in the amplitude and phase [35]. These waveforms include the effects of periastron precession, the precession of the orbital plane due to spin-orbit coupling, and higher harmonics from the higher order mass and current multipole moments. Our waveform model does not include the effects of spin-spin coupling which enter at 2PN order. In future work we plan to extend the waveform model and our parameter estimation study to higher Post-Newtonian order.

The fastest time scale for the system is the orbital time scale, which to leading order is given by Kepler's law:

$$T_{\mathrm{orb}} \sim 2\pi a^{\frac{3}{2}} M^{-\frac{1}{2}} \tag{1}$$

where $M = m_1 + m_2$ is the total mass of the system and a is the semi-major axis. Periastron advance enters at $1\,\mathrm{PN}$ order, with a fractional advance per orbit of $k = 3M^2\mu^2/L^2$, where $\mu = m_1 m_2/M$ is the reduced mass of the system, $L \simeq \mu\sqrt{aM(1-e^2)}$ is the orbital angular momentum and e is the eccentricity of the orbit. The ratio of the periastron precession timescale to the orbital timescale is given by

$$\frac{T_{\mathrm{peri}}}{T_{\mathrm{orb}}} = \frac{2\pi}{k} \simeq \frac{a}{M} \,. \tag{2}$$

The orbital angular momentum $\mathbf{L}$ precesses with angular velocity $\boldsymbol{\omega}_{\mathrm{prec}} = \mathbf{S}_{\mathrm{eff}}/r^3$ [35], where

$$\mathbf{S}_{\mathrm{eff}} = 2\left(1 + \frac{3m_2}{4m_1}\right)\mathbf{S}_1 + 2\left(1 + \frac{3m_1}{4m_2}\right)\mathbf{S}_2 \tag{3}$$

The effective spin vector has magnitude $S_{\mathrm{eff}} \sim M^2$ since the magnitude of the individual spins is given by $S_i = \chi_i m_i^2$ where the dimensionless spin parameter $0 \leq \chi_i \leq 1$. The ratio of the precession time scale and the orbital timescale is given by

$$\frac{T_{\mathrm{prec}}}{T_{\mathrm{orb}}} \sim \left(\frac{a}{M}\right)^{\frac{3}{2}} \,. \tag{4}$$

We see that the precession of the orbital plane enters at $1.5\,\mathrm{PN}$ order relative to the orbital time scale. The precession of the orbital angular momentum due to spin-orbit coupling results in a modulation of the amplitude of the gravitational waveform at the solar system barycenter.
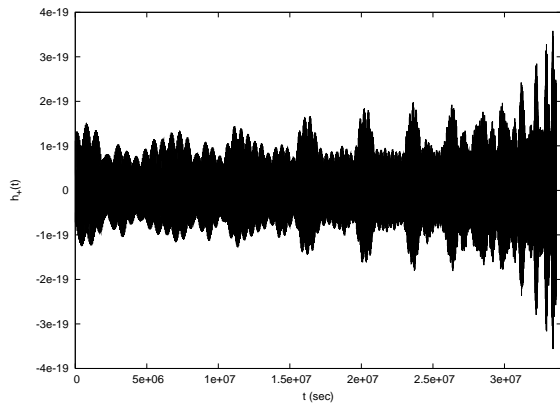
FIG. 2: The time dependent gravitational waveform $h_+(t)$ at the solar system barycenter for a binary black hole system with $e_0 = 0.3$ (Source 1 in Table II) during the final year before merger.

The rate at which the binary black hole system loses energy and angular momentum due to gravitational wave emission defines the decay time scale

$$T_{\text{decay}} \sim \frac{E}{\dot{E}} \sim \frac{L}{\dot{L}} \qquad (5)$$

and the ratio

$$\frac{T_{\text{decay}}}{T_{\text{orb}}} \sim \frac{M}{\mu} \left(\frac{a}{M}\right)^{\frac{5}{2}} . \qquad (6)$$

The loss of energy and angular momentum results in the decay of the semi-major axis and the radial eccentricity of the system. Orbit averaged expression for these decay rates can be found in Ref. [35]. The effects of spin-orbit induced precession of the orbital plane and the overall sweep up in frequency and amplitude as the system inspirals over the course of a year are apparent in Figure 2 for a system with $e_0 = 0.3$ and other source parameters given in Table II for Source 1.

At times well before the merger of the system M/a is small and we find that

$$T_{\text{decay}} > T_{\text{prec}} > T_{\text{peri}} > T_{\text{orb}} . \qquad (7)$$

We take advantage of this separation of the relevant time scales to make our waveform calculations more efficient. Since the decay and precession timescales are much longer than the orbital timescale we can start with a solution to the orbital equations of motion that neglects dissipation. This allows us to use Nyquist sampling of just a couple of samples per orbit for the quantities that depend on the dissipation and precession equations and saves considerable computational cost. Considering only times early in the evolution of the system we have a clean separation of time scales and the different processes can be treated differently in the calculations. This simplifies the problem by allowing an adiabatic treatment where the dissipation is assumed to be small over the course

of an orbit and the eccentricity and semi-major axis are treated as constant while calculating an individual orbit.

The approximations involved in exploiting the separation of timescales introduce small errors in the waveforms. The largest of these comes from using the orbit-averaged spin precession equations, which neglects small periodic changes in the spin orientations that occur on the orbital timescale, but these changes are effectively 2.5 PN order contributions to the higher harmonics. The averaging also introduces small errors in the long term secular evolution that scale as the ratio of the averaging time scale (in our case the orbital timescale) and the timescale of the terms being averaged (such as the spin precession timescale). These errors are multiplicative, and so represent higher PN order terms that can be discarded at 1.5 PN order.

As the system approaches merger the various time scales become comparable and our waveform model breaks down. We adopt the termination condition $2\pi M f_{\text{orb}} = 0.01$, which corresponds to an expansion parameter $M/a \approx 0.05$. Denoting the time when this condition is met as t_s, and the orbital frequency at this time as f_s, we taper the waveform smoothly to zero by multiplying the waveform with a half-Hann filter:

$$w(t) = \begin{cases} 1, & \text{if } t \leq t_H \\ \cos^2\left(\pi(t - t_H)f_s/3\right), & \text{if } t > t_H \end{cases} \qquad (8)$$

with $t_H = t_s - 3/(2f_s)$.

Our termination condition is conservative in terms of the signal to noise ratio (SNR) LISA will be able to extract from this type of source. Most of the SNR comes from times near merger, so the extension of the validity of the waveform closer to merger results in a big increase in SNR. Our study here is thus a pessimistic estimate of how well LISA will be able to determine the various source parameters. In the case of the radial eccentricity parameter however, the circularization of the waveform toward merger means that most of the eccentricity information is encoded at times well before merger. While increased SNR would improve the determination of the other source parameters, we find that the eccentricity is not highly correlated with the other parameters (see Figure 13). Our choice for when to truncate the waveform thus should not have much of an effect on our study of how well LISA will be able to determine the eccentricity of black hole binary systems.

We have tested our waveform generator in various limits against other codes. In the circular limit, and with dissipation turned off, we found precise agreement with the 1.5 PN limit of the spinning black hole code developed by Cornish, Hughes, Lang and Nissanke that is described in Ref. [37]. We do not expect, and nor do we find, precise agreement when dissipation is included. This is because our eccentric waveform generator evolves the semi-major axis, while the circular orbit code evolves the orbital frequency, which leads to numerical differences at 2 PN order. In the 0-PN limit (hence no spin effects and no

higher harmonics) we find precise agreement with the Peters and Matthews waveforms [7].

III. LISA RESPONSE

We simulate the LISA response to a gravitational wave signal plus instrument noise and confusion noise due to galactic binary sources of gravitational waves. We adopt the standard ecliptic coordinate system with origin at the barycenter. The individual data streams from the six LISA phase meters can be combined to cancel out the laser phase noise and form Time Delay Interferometry (TDI) variables [38]. The Michelson style TDI variables $\{X, Y, Z\}$ can be used to construct three noise orthogonal data streams that are similar to the $\{A, E, T\}$ variables described in Ref. [39].

Processing the gravitational waveform through the LISA response function imparts additional amplitude and frequency modulations on the one year timescale of the LISA orbits. These effects can be seen in Figure 3, which shows the A-channel response to the Barycenter signal shown previously in Figure 2.
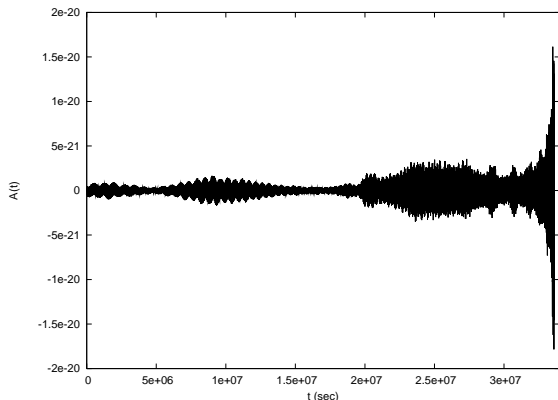

FIG. 3: The $A(t)$ channel response to the spinning binary black hole system shown in Figure 2. The amplitude modulation is due to a combination of the antenna pattern sweeping around as LISA orbits the Sun, and the spin induced precession of the orbital plane. The overall gravitational wave amplitude grows as the system spirals in and nears merger.

The one-sided noise spectral density of the detector in the A and E channels is given by [41]:

$$S_{\text{inst}}(f) = \frac{4}{3} [(2 + \cos u)S_n^p(f) + 4 \left(1 + \cos u + \cos^2 u\right) \frac{S_n^a(f)}{(2\pi f)^4}], \quad (9)$$

where $u = 2\pi f/L$, $S_n^p(f)$ is the position noise and $S_n^a(f)$ is acceleration noise, and we have taken the limit of symmetric noise in the detector. The confusion noise due to gravitational wave sources in the galaxy has been estimated by direct simulation of the LISA response [43]

to a synthetic galaxy [42], followed by the removal of resolvable systems [44]. An approximate fit to the resulting confusion noise estimate is given by

$$S_{\text{conf}}(f) = \begin{cases} 10^{-44.8} f^{-2.4} & 10^{-4} < f < 4.5 \times 10^{-4} \\ 10^{-47.15} f^{-3.1} & 4.5 \times 10^{-4} < f < 1.1 \times 10^{-3} \\ 10^{-51} f^{-4.4} & 1.1 \times 10^{-3} < f < 1.7 \times 10^{-3} \\ 10^{-74.7} f^{-13} & 1.7 \times 10^{-3} < f < 2.5 \times 10^{-3} \\ 10^{-59.15} f^{-7} & 2.5 \times 10^{-3} < f < 4 \times 10^{-3} \end{cases}.$$
$$(10)$$

The total noise is then taken to be the sum of the the two contributions: $S_n(f) = S_{\text{inst}}(f) + S_{\text{conf}}(f)$.

IV. PARAMETER ESTIMATION

The goal of a parameter estimation study is to find how accurately we can determine the values of the source parameters for a given signal. We take a Bayesian approach and use the Markov Chain Monte Carlo (MCMC) technique to compute the posterior distribution function $p(\vec{x}|s)$ describing the model parameters $\vec{x}$ that we infer from data s. Our results establish how well the various source parameters will be able to be determined by the LISA mission, including the orbital eccentricity.

The use of MCMC techniques in gravitational wave data analysis is now a familiar technique for parameter estimation in gravitational wave astronomy [45–50]. The result of a well constructed MCMC is a set of samples from the posterior distribution. The number of samples from a particular region of parameter space is proportional to the posterior weight contained in that region. The uncertainty in each parameter is given by quantiles of the marginalized posterior distribution (e.g. the half-width of the 90th percentile equates to a 2-σ error if the distributions are Gaussian).

By Bayes theorem, the posterior distribution is given by the product of the prior distribution $p(\mathbf{x})$ and likelihood $p(s|\mathbf{x})$, normalized by the evidence $p(s) = \int p(\mathbf{x})p(\mathbf{x}|s) \, d\mathbf{x}$. For Gaussian noise, the likelihood of the data s having being generated by a gravitational wave signal $h(\mathbf{x})$ is given by

$$p(s|\mathbf{x}) = Ce^{-\frac{1}{2}(s-h(\mathbf{x})|s-h(\mathbf{x}))} , \quad (11)$$

where C is a normalization constant that does not depend on the signal or the template. Here we have used the noise weighted inner product

$$(a|b) = 2 \int_0^\infty \frac{a^*(f)b(f) + a(f)b^*(f)}{S_n(f)} \, df , \quad (12)$$

where $S_n(f)$ is the one-sided noise spectral density. The prior probability density for $\mathbf{x}$ reflects our knowledge of the source parameter, however ill-formed, before we analyze the data. For example, we assume a uniform prior for angular parameters such as the sky location and the initial orientation of the angular momentum vector, such

that the cosine of the co-latitude is uniformly distributed in the range $[-1 : 1]$ and the azimuth is uniformly distributed in the range $[0 : 2\pi]$.

The primary mode of the posterior distribution yields the best fit values for the source parameters, according to the current data and our prior knowledge. In many instances the posterior distribution is multi-modal, and the quantiles used to estimate the parameter uncertainties may cover disjoint regions in parameter space. Even when the bulk of the posterior weight lies in a single, contiguous region, the posterior distribution may not be well approximated by a Gaussian distribution. Nonetheless, a Gaussian approximation to the posterior distribution often provides a reasonable estimate of the parameter estimation errors, which can be efficiently computed using the Fisher information matrix Γ_{ij}, which measures the expectation value of the curvature of the posterior distribution about the mode:

$$\Gamma_{ij} = -\langle \partial_i \partial_j \ln p(\mathbf{x}|s) \rangle|_{\text{mode}}. \tag{13}$$

We employ a parallel tempered [52] Metropolis-Hastings [53, 54] MCMC routine to explore the PDF. The Markov chain starts at parameter values $\mathbf{x}$ and transitions to $\mathbf{y}$ with probability

$$H = \min \left[\frac{p(\mathbf{y})p(s|\mathbf{y})q(\mathbf{x}|\mathbf{y})}{p(\mathbf{x})p(s|\mathbf{x})q(\mathbf{y}|\mathbf{x})}, 1 \right]. \tag{14}$$

Here $q(\mathbf{x}|\mathbf{y})$ is the proposal distribution, which is the function that generates proposals for moves from $\mathbf{x}$ to $\mathbf{y}$. The performance of an MCMC algorithm is quite sensitive to the choice of proposal distribution, and care must be taken to ensure that the chains do not get stuck on local maxima of the PDF. We employed several techniques to ensure rapid exploration of the full parameter space: local coordinate transformations to uncouple the parameters; moves that exploit symmetries of the likelihood surface to encourage jumps between local maxima; and parallel tempering to encourage wide exploration of the posterior [50, 51, 56]. The number of iterations spent at each parameter value is proportional to the posterior density, and histograms of the parameters visited by the chain provide an estimate of the posterior distribution.

We have found that drawing from a variety of proposal distributions provides a set of jump proposals that tend to produce an MCMC that efficiently maps out the desired PDF and provides accurate parameter uncertainties even for very large search spaces. Our parameter estimation study thus uses several proposal distributions, including parallel tempering and Fisher matrix proposals. In this high dimensional parameter space we found it advantageous to use the Fisher matrix approximation to the posterior to propose jumps along single eigen-directions as part of the mixture of jump proposals.

V. PARAMETER ESTIMATION WITH LISA

We can use our time dependent gravitational waveforms [35] and established MCMC techniques to study how well LISA will be able to measure the full set of seventeen parameters necessary to describe a spinning binary black hole system in an eccentric orbit. We are especially interested in determining when eccentric orbits can be distinguished from circular orbits.

We chose to study signals in their final year prior to merger, with an observation time that extends just beyond the merger. In order to choose initial parameter values for a system that will merge in one year, we need to calculate an initial semi-major axis based on the lifetime estimate for a system with some given initial radial eccentricity. We use the leading order, 0 PN expression for a_0 [8]

$$a_0 = 4 \left(\frac{\mu M^2}{5} T_c \right)^{\frac{1}{4}} \left(1 + \frac{157}{172} e_0^2 + \frac{5799977}{7336832} e_0^4 + \frac{1888175763}{2523870208} e_0^6 \right), \tag{15}$$

as an initial guess, and apply a bisection routine to the full numerical orbital evolution to find the value of a_0 that yields a merger time T_c of one year.

TABLE I: Parameter ranges for our study of spinning black hole binary systems in eccentric orbits.

Parameter	Minimum	Maximum
m_1	$10^5 M_\odot$	$10^7 M_\odot$
m_2	$10^5 M_\odot$	$10^7 M_\odot$
D_L	1 Gpc	100 Gpc
e_0	0	1
a_0	20 M	1000 M
χ_1	0	1
χ_2	0	1
$\cos\theta$	-1	1
$\cos\theta_L$	-1	1
$\cos\theta_{S_1}$	-1	1
$\cos\theta_{S_2}$	-1	1
ϕ	0	2π
ϕ_L	0	2π
ϕ_{S_1}	0	2π
ϕ_{S_2}	0	2π
n_0	0	2π
ϕ_0	0	2π

We use parameter ranges consistent with typical LISA sources, given in Table I. The masses are given in terms of the mass of the Sun, $M_\odot = 1.9891 \times 10^{30}$ kg, and the luminosity distance D_L is given in units of Gigaparsecs. The dimensionless spin parameters χ_1 and χ_2

combine with the black hole masses to give the magnitudes of the spins, $S_i = \chi_i m_i^2$. There are initial orientation parameters for the orbital angular momentum vector $\mathbf{L} \rightarrow (\cos\theta_L, \phi_L)$, as well as the spin vectors $\mathbf{S}_i \rightarrow (\cos\theta_{S_i}, \phi_{S_i})$. The final two parameters, n_0 and ϕ_0, are initial phases related to the mean motion and orbital phase. In the circular limit these parameters are degenerate, but for eccentric orbits we have to specify the initial periastron position. In the present study we have ignored the possibility that gas dynamics may partially aligned the spins with the orbital angular momentum [57], which would restrict the prior ranges and reduce the degree of orbital precession. The impact of this partial alignment on parameter estimation has been considered for circular orbits [58], and it would be interesting to extend this study to include eccentricity.

Here we study several representative cases to establish the parameter recovery errors and to study correlations between the parameters. The high dimension of the parameter space makes it difficult to perform a comprehensive study - if we were to choose just two values of each parameter we would need to perform $2^{17} \sim 10^5$ parameter estimation studies. Each MCMC run involves $\sim 100,000$ iterations with ~ 8 parallel chains, and takes about a week to run on a single 2.66 GHz Intel processor, so we are limited in the number of examples we can consider. We perform MCMC parameter estimation studies of several representative examples, varying the mass ratio, sky location, distance, eccentricity, and dimensionless spin parameters. We only looked at a few initial spin and orbital orientations since we do not expect these to have a significant effect on the results - unless the initial orientations are very special the system will explore a wide range of orientations during the orbital evolution. To be able to explore the parameter space more widely would take a faster code. One possibility is to use the Fisher information matrix approximation to the posterior, which is many orders of magnitude faster than a full MCMC study. In preparation for such a study we compare the Fisher matrix approximation to the MCMC derived posterior distributions and find that the approximation is fairly reliable so long as the initial eccentricity exceeds $e_0 \sim 0.01$.

Our first study focuses on determining when the eccentricity one year before merger is distinguishable from zero. We studied two systems that only differed in sky location (and hence in SNR), and considered initial eccentricities in the range $e_0 \in [0.001, 0.2]$, see Table II for a list of the other source parameters. Marginalized posterior distributions for e_0 are shown in Figure 4 for Source 1, and Figure 5 for Source 2. We see that the error in the measured value of e_0 gets smaller as e_0 gets larger, but the dependence on e_0 is fairly weak, and never larger than $\Delta e_0 \sim 0.001$. Our criteria for deciding if the eccentricity is distinguishable from zero is to see if their is any weight in the posterior distribution at $e_0 = 0$ (this test is motivated by the Savage-Dicke density ratio estimate for the model evidence [43]). For Source 1 we see that the ex-

TABLE II: Injected parameter values for two sets of sources studied with a range of values for e_0. The results of the parameter estimation study for Source 1 are given in Figure 4 and the results for Source 2 are given in Figure 5.

Parameter	Source 1	Source 2
m_1	$2 \times 10^6 M_\odot$	$2 \times 10^6 M_\odot$
m_2	$1 \times 10^6 M_\odot$	$1 \times 10^6 M_\odot$
D_L	6.36167 Gpc	6.36167 Gpc
χ_1	0.5	0.5
χ_2	0.8	0.8
$\cos\theta$	0.2	0.4
$\cos\theta_L$	-0.5	-0.5
$\cos\theta_{S_1}$	-0.8	-0.8
$\cos\theta_{S_2}$	0.6	0.6
ϕ	1.2	2.0
ϕ_L	2.6	2.6
ϕ_{S_1}	0.4	0.4
ϕ_{S_2}	1.7	1.7
n_0	0.2	0.2
ϕ_0	1.65	1.65

amples with $e_0 \geq 0.005$ are clearly distinguishable from circular, while the $e_0 = 0.002$ case is on the margin of detectability. For Source 2, which has higher SNR due to a more favorable sky location, the $e_0 = 0.002$ case is clearly distinguishable from circular. The Fisher matrix approximation to the posterior distribution is computed at the maximum a posteriori probability (MAP) value of the parameters, and is found to work well for eccentricities $e_0 > 0.05$, but breaks down for small eccentricities. The MCMC derived posterior distributions are much flatter than a Gaussian distribution, and we attribute the failure of our Fisher matrix estimates to only including the leading order, quadratic curvature terms in the Fisher matrix calculation.

This study suggests that LISA observations of eccentric black hole binary systems will be able to measure the eccentricity of the system and distinguish eccentric systems from circular systems to parts in a thousand. A similar study was performed by Porter and Sesana [27] for non-spinning eccentric binary black hole systems. Their results suggest that LISA will be able to measure the eccentricity to parts in 10^{-4} for such sources.

We find that the other source parameters are also measured quite well, as illustrated in Figure 6 and Figure 7. Marginalized posterior distributions are shown for the chirp mass $M_c = (m_1 m_2)^{3/5}/(m_1 + m_2)^{1/5}$ and reduced mass $\mu = m_1 m_2/(m_1 + m_2)$, the distance to the source, the initial radial eccentricity, and the two sky location parameters. We compare the Fisher matrix approximation to the marginalized posterior distributions computed from the MCMC runs and find excellent agreement for all the parameters (except for the eccentricity in Figure 6).
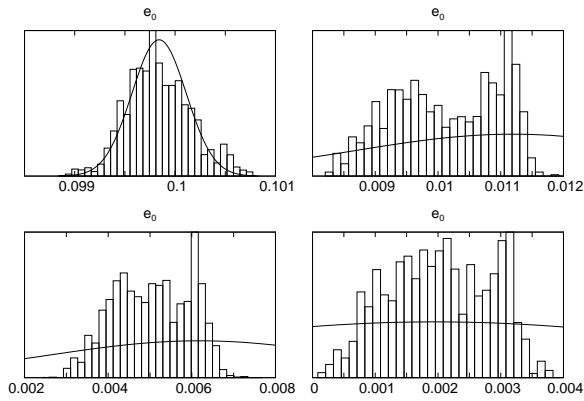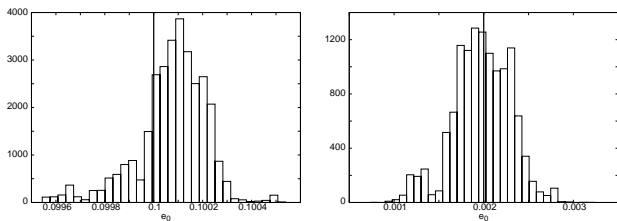
FIG. 4: Marginalized posterior distribution for the initial radial eccentricity for sources with the same parameter values except for different initial eccentricities and semi-major axes. The boxed histograms are derived from the Markov chains, while the solid lines are the Fisher matrix predictions computed at the MAP values of the parameters (which are pushed off the true values by the instrument noise). Top left $e_0 = 0.1$, $a_0 = 69.96M$, SNR= 231; top right $e_0 = 0.01$, $a_0 = 68.33M$, SNR= 237; bottom left $e_0 = 0.005$, $a_0 = 69.3M$, SNR= 237; bottom right $e_0 = 0.002$, $a_0 = 69.3M$, SNR= 237. The other parameter values correspond to Source 1 in Table II.

FIG. 5: The marginalized posterior distribution for the initial radial eccentricity for sources with the same parameter values except for different initial eccentricities and semi-major axes. On the left $e_0 = 0.1$, $a_0 = 68.94M$, SNR= 557; on the right $e_0 = 0.002$, $a_0 = 68.32M$, SNR= 559. For this source, $e_0 = 0.002$ is distinguishable from the circular case. A vertical line marks the injected e_0 value in each plot. The other parameter values are given in Table II, Source 2.

As a start to exploring the large parameter space of eccentric binary black hole systems we consider a few representative examples below. We find that in general physical parameters are well constrained by LISA observations and that the Fisher matrix makes fair estimates of the parameter errors. In addition to the examples below with varied spin and distance parameters we also studied systems with a range of mass ratios $m_1/m_2 \in [1, 5]$ and total masses $M \in [10^5 M_\odot, 10^7 M_\odot]$ with similar results. We also compared the parameter estimation errors with those obtained when the eccentricity is held fixed at zero, and saw only small (less than 50%) changes in the error estimates.

The dimensionless spin parameters χ_1 and χ_2 are varied in Table III to study the cases of large and small spin
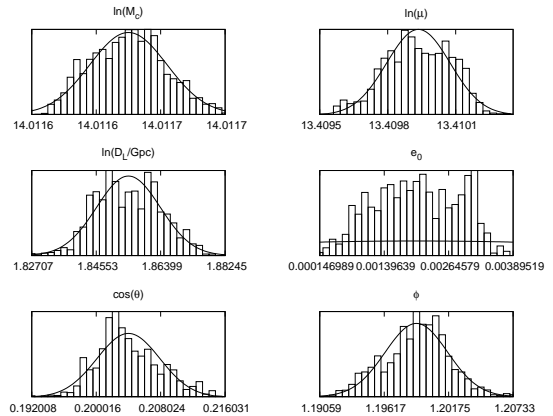

FIG. 6: The marginalized posterior distribution for several source parameters, including the initial radial eccentricity with injected value $e_0 = 0.002$, $a_0 = 69.3M$, and SNR= 237. The other injected source parameters are those of Source 1 in Table II. The solid lines are the Fisher matrix predictions computed at the MAP values of the parameters.
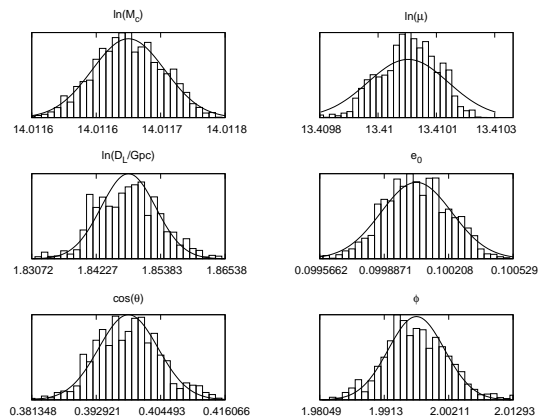

FIG. 7: The marginalized posterior distribution for several source parameters, including the initial radial eccentricity with injected value $e_0 = 0.1$, $a_0 = 68.94M$, and SNR = 558. The other injected source parameters are those of Source 2 in Table II. The solid lines are the Fisher matrix predictions computed at the MAP values of the parameters.

parameters. The magnitude of the spin vectors is related to the mass of the black hole $S_i = \chi_i m_i^2$. The posterior distribution for several of the source parameters for these cases are given in Figures 8 and 9. The Fisher approximation is a reasonable prediction of the width of the posterior distribution for the spin of the more massive body, but does a poor job for the less massive body. This discrepancy was seen in many other examples that we looked at. The cause of the discrepancy is presently not understood. Two lower SNR examples are shown in Figure 10 and Figure 11, and we see good agreement with the Fisher matrix estimates.

We do not expect the eccentricity to be highly corre-

TABLE III: Source 3 gives the injected parameter values for Figure 8 with large spin values. Source 4 gives the injected parameter values for Figure 9 with small spin values.

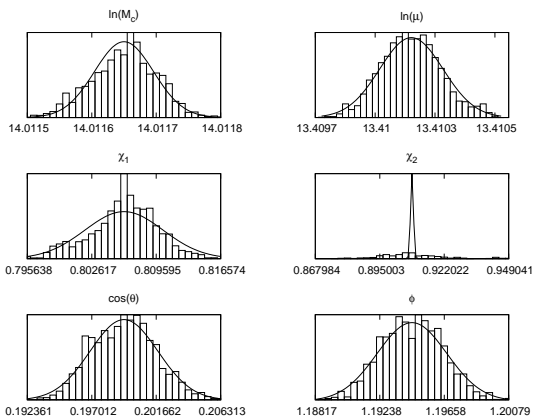| Parameter	Source 3	Source 4
m_1	$2 \times 10^6 M_\odot$	$2 \times 10^6 M_\odot$
m_2	$1 \times 10^6 M_\odot$	$1 \times 10^6 M_\odot$
D_L	6.36167 Gpc	6.36167 Gpc
e_0	0.1	0.1
a_0	68.96 M	68.91 M
χ_1	0.8	0.1
χ_2	0.9	0.11
$\cos\theta$	0.2	0.2
$\cos\theta_L$	-0.5	-0.5
$\cos\theta_{S_1}$	-0.8	-0.8
$\cos\theta_{S_2}$	0.6	0.6
ϕ	1.2	1.2
ϕ_L	2.6	2.6
ϕ_{S_1}	0.4	0.4
ϕ_{S_2}	1.7	1.7
n_0	0.2	0.2
ϕ_0	1.65	1.65
SNR	250	197

FIG. 8: The marginalized posterior distribution for several source parameters for Source 3 in Table III. The solid lines are the Fisher matrix predictions computed at the MAP values of the parameters.
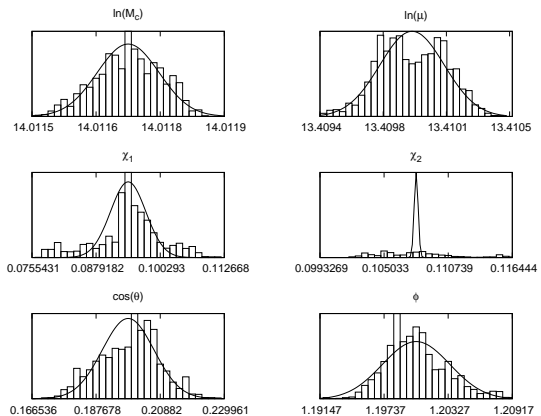

FIG. 9: The marginalized posterior distribution for several source parameters for Source 4 in Table III. The solid lines are the Fisher matrix predictions computed at the MAP values of the parameters.

TABLE IV: Source 5 gives the injected parameter values for Figure 10 with redshift $z \sim 1.5$. Source 6 gives the injected parameter values for Figure 11 with redshift $z \sim 2$.

Parameter	Source 5	Source 6
m_1	$2 \times 10^6 M_\odot$	$2 \times 10^6 M_\odot$
m_2	$1 \times 10^6 M_\odot$	$1 \times 10^6 M_\odot$
D_L	11.008 Gpc	15.733 Gpc
e_0	0.1	0.1
a_0	68.94 M	68.94 M
χ_1	0.5	0.8
χ_2	0.5	0.8
$\cos\theta$	0.2	0.2
$\cos\theta_L$	-0.5	-0.5
$\cos\theta_{S_1}$	-0.8	-0.8
$\cos\theta_{S_2}$	0.6	0.6
ϕ	1.2	1.2
ϕ_L	2.6	2.6
ϕ_{S_1}	0.4	0.4
ϕ_{S_2}	1.7	1.7
n_0	0.2	0.2
ϕ_0	1.65	1.65
SNR	132	92

lated with the other source parameters since the higher harmonics introduced in the waveform due to eccentricity cannot be simulated by changes in other parameters or their combinations. We indeed find that the initial eccentricity is not correlated with the other parameters. Compare the distribution of values for the two masses in Figure 12 to the distribution of mass and eccentricity values in Figure 13. The two masses are highly correlated since it is the total mass of the system and the ratio of

the masses that appear in the waveform. The distribution of eccentricity versus the other source parameters is similar to that seen in Figure 13.

VI. CONCLUSION

Our studies of the response of the LISA detector to the gravitational wave signal from spinning binary black
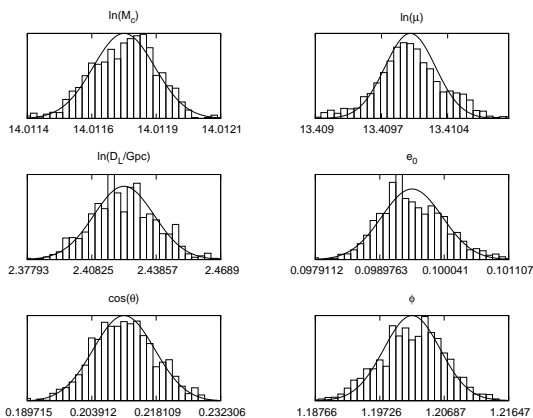
FIG. 10: The marginalized posterior distribution for several parameters for a source with $z \sim 1.5$ $e_0 = 0.1$, and SNR = 132 (Table IV, Source 5). The solid lines are the Fisher matrix predictions computed at the MAP values of the parameters.

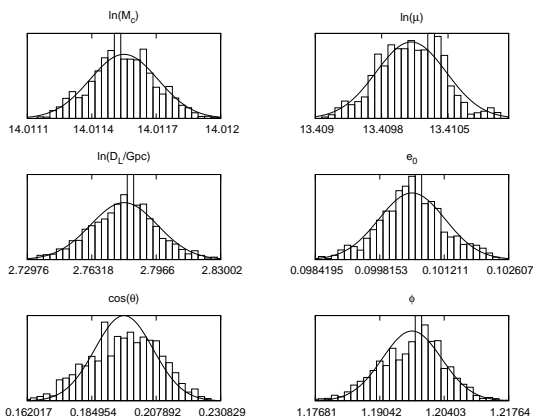FIG. 11: The marginalized posterior distribution for several parameters for a source with $z \sim 2$, $e_0 = 0.1$, and SNR = 92 (Table IV, Source 6). The solid lines are the Fisher matrix predictions computed at the MAP values of the parameters.
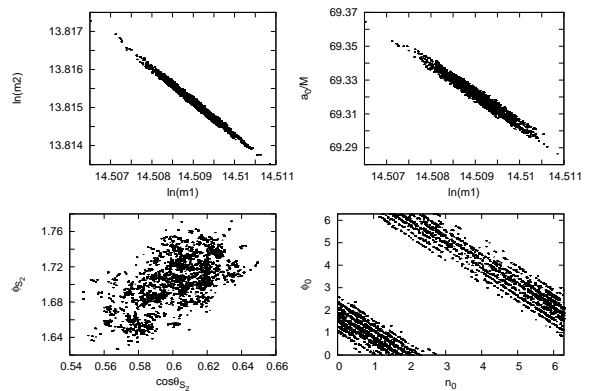

FIG. 12: Two dimensional posterior distribution scatter plots showing the correlation between pairs of parameters for a source with initial radial eccentricity $e_0 = 0.002$ and SNR = 237 (Table II, Source 1). Upper left m_1 and m_2, upper right m_1 and a_0, bottom left $\cos\theta_{S_2}$ and ϕ_{S_2}, bottom right n_0 and ϕ_0.
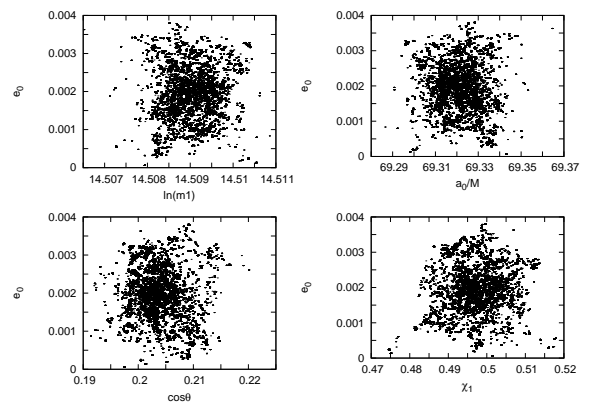

FIG. 13: Two dimensional posterior distribution scatter plots for a source with initial radial eccentricity $e_0 = 0.002$ and SNR = 237 (Table II, Source 1). Upper left m_1 and e_0, upper right a_0 and e_0, bottom left $\cos\theta$ and e_0, bottom right χ_1 and e_0.

hole systems in eccentric orbits show that the eccentricity should not be neglected for LISA data analysis and parameter estimation. We find that LISA can determine the eccentricity of the system one year before merger to parts in a thousand. This result depends only weakly on the initial value of the eccentricity, indicating that LISA will be able to distinguish between eccentric and circular orbits at the same level $(e_0 \sim 10^{-3})$.

The construction of the gravitational waveforms for spinning binary black hole systems in eccentric orbits to 1.5 PN order in [35] establishes the framework for the extension of this work to higher post-Newtonian order. Binary black hole waveforms that include eccentricity will be necessary for several of the LISA science goals including constraining galaxy merger scenarios and testing general relativity in the strong field regime near supermassive black holes.

This work builds the foundation for further studies including a comprehensive exploration of the parameter space including source sky location, distance, spins, masses, and mass ratios. For sources with initial radial eccentricity greater than $e_0 \sim 0.02$ the Fisher matrix is a good approximation to the posterior distribution. The very large parameter space could be studied quickly using the Fisher approximation, although it is not as useful for the low initial eccentricity cases.

The equations of motion and instantaneous gravitational waveforms have been calculated to the next post-Newtonian order and these pieces can be included in a future parameter estimation study. The 2 PN effects include the spin-spin coupling of the two black holes and thus corrections to the precession and evolution of the system.

These waveforms can be also be used to study how well

the Advanced LIGO-Virgo network and proposed Einstein Telescope will be able to measure eccentricity and what level of bias could be expected from using circular templates for parameter estimation.

VII. ACKNOWLEDGMENTS

[1] M. Micic, K. Holley-Bockelmann, S. Sigurdsson, and T. Abel, Mon. Not. Roy. Astron. Soc. **380**, 1533 (2007), astro-ph/0703540.

[2] A. Sesana, M. Volonteri, and F. Haardt, Mon. Not. Roy. Astron. Soc. **377**, 1711 (2007), astro-ph/0701556.

[3] J. Kormendy and D. Richstone, Ann. Rev. Astron. Astrophys. **33**, 581 (1995).

[4] J. Magorrian et al., Astron. J. **115**, 2285 (1998), astro-ph/9708072.

[5] R. Narayan, New Journal of Physics **7**, 199 (2005),

[6] M. C. Begelman, R. D. Blandford, and M. J. Rees, Nature **287**, 307 (1980).

[7] P. C. Peters and J. Mathews, Phys. Rev. **131**, 435 (1963).

[8] P. C. Peters, Physical Review **136**, 1224 (1964).

[9] A. Krolak and B. F. Schutz, General Relativity and Gravitation **19**, 1163 (1987).

[10] M. Colpi, L. Mayer, and F. Governato, arXiv **astro-ph/9907088** (1999), astro-ph/9907088.

[11] K. Gultekin, M. Coleman Miller, and D. P. Hamilton, Astrophys. J. **640**, 156 (2006), astro-ph/0509885.

[12] M. Dotti, M. Colpi, and F. Haardt, arXiv **astro-ph/0602013** (2006), astro-ph/0602013.

[13] P. Berczik, D. Merritt, and R. Spurzem, Astrophys. J. **633**, 680 (2005), astro-ph/0507260.

[14] P. J. Armitage and P. Natarajan, Astrophys. J. **634**, 921 (2005), astro-ph/0508493.

[15] S. J. Aarseth, Astrophys. Space Sci. **285**, 367 (2003), astro-ph/0210116.

[16] P. Amaro-Seoane and M. Freitag, Astrophys. J. **653**, L53 (2006) [arXiv:astro-ph/0610478].

[17] P. Amaro-Seoane, J. R. Gair, M. Freitag, M. Coleman Miller, I. Mandel, C. J. Cutler and S. Babak, Class. Quant. Grav. **24**, R113 (2007) [arXiv:astro-ph/0703495].

[18] P. Amaro-Seoane, C. Miller and M. Freitag, Astrophys. J. **692**, L50 (2009) [arXiv:0901.0604 [astro-ph.SR]].

[19] P. Amaro-Seoane, C. Eichhorn, E. Porter and R. Spurzem, arXiv:0908.0755 [astro-ph.GA].

[20] A. Sesana, arXiv:1006.0730 [astro-ph.CO]

[21] J. E. Plowman, D. C. Jacobs, R. W. Hellings, S. L. Larson and S. Tsuruta, "Constraining the Black Hole Mass Spectrum with Gravitational Wave Observations I: The Error Kernel" arXiv:0903.2059 [astro-ph].

[22] A. Sesana, J. R. Gair, E. Berti and M. Volonteri, arXiv:1011.5893 [astro-ph.CO].

[23] J. E. Plowman, R. W. Hellings and S. Tsuruta, arXiv:1009.0765 [astro-ph.CO].

[24] K. Martel and E. Poisson, Physical Review D **60**, 124008 (1999),

[25] D. A. Brown and P. J. Zimmerman, Phys. Rev. **D81**, 024007 (2010), 0909.0066.

[26] C. Cutler and M. Vallisneri, Phys. Rev. **D76**, 104018 (2007), 0707.2982.

[27] E. K. Porter and A. Sesana, "Eccentric Massive Black Hole Binaries in LISA I : The Detection Capabilities of Circular Templates," arXiv:1005.5296 [gr-qc].

[28] L. E. Kidder, Phys. Rev. **D52**, 821 (1995), gr-qc/9506022.

[29] G. Faye, L. Blanchet and A. Buonanno, "Higher-order spin effects in the dynamics of compact binaries. I: Equations of motion," Phys. Rev. D **74**, 104033 (2006)

[30] L. Blanchet, A. Buonanno and G. Faye, "Higher-order spin effects in the dynamics of compact binaries II. Radiation field," Phys. Rev. D **74**, 104034 (2006)

[31] J. Majar and M. Vasuth, Phys. Rev. **D77**, 104005 (2008), 0806.2273.

[32] Nicolas Yunes and Frans Pretorius "Fundamental Theoretical Bias in Gravitational Wave Astrophysics and the Parameterized Post-Einsteinian Framework" Phys. Rev. D **80**, 122003 (2009)

[33] L. Wen, The Astrophysical Journal **598**, 419 (2003)

[34] R. M. O'Leary, B. Kocsis, and A. Loeb, MNRAS (2009),

[35] N. J. Cornish and J. S. Key, Phys. Rev. D **82**, 044028 (2010) arXiv:1004.5322 [gr-qc].

[36] R. N. Lang and S. A. Hughes, Phys. Rev. D **74**, 122001 (2006) [Erratum-ibid. D **75**, 089902 (2007 ERRAT,D77,109901.2008)] [arXiv:gr-qc/0608062].

[37] K. G. Arun et al., Class. Quant. Grav. **26**, 094027 (2009) [arXiv:0811.1011 [gr-qc]].

[38] F. B. Estabrook, M. Tinto, and J. W. Armstrong, Phys. Rev. D **62** (2000).

[39] T. A. Prince, M. Tinto, S. L. Larson, and J. Armstrong, Phys. Rev. D **66** (2002).

[40] N. J. Cornish, "Detecting a stochastic gravitational wave background with the laser interferometer space antenna," Phys. Rev. D **65**, 022004 (2002)

[41] M. R. Adams and N. J. Cornish, "Discriminating between a Stochastic Gravitational Wave Background and Instrument Noise," arXiv:1002.1291 [gr-qc].

[42] G. Nelemans, L. R. Yungelson and S. F. Portegies Zwart, "The gravitational wave signal from the galactic disk population of binaries containing two compact objects," A&A 375 3 890-898 (2001)

[43] N. J. Cornish and T. B. Littenberg, Phys. Rev. D **76**, 083006 (2007)

[44] J. Crowder and N. Cornish, Phys. Rev. D **75**, 043008 (2007)

[45] N. Christensen and R. Meyer, "Markov chain Monte Carlo methods for Bayesian gravitational radiation data analysis," Phys. Rev. D **58**, 082001 (1998)

[46] N. Christensen and R. Meyer, "Using Markov chain Monte Carlo methods for estimating parameters with gravitational radiation data," Phys. Rev. D **64**, 022001 (2001)

[47] N. J. Cornish and J. Crowder, Phys. Rev. D **72**, 043005 (2005) [arXiv:gr-qc/0506059].

[48] N. J. Cornish and E. K. Porter, Class. Quant. Grav. **23**, S761 (2006), gr-qc/0605085.

[49] T. B. Littenberg and N. J. Cornish, Phys. Rev. D **80**, 063007 (2009) [arXiv:0902.0368 [gr-qc]].

[50] M. van der Sluys et. al., Class. Quant. Grav. **25**, 184011 (2008), 0805.1689.

[51] J. S. Key and N. J. Cornish, Phys. Rev. **D79**, 043014 (2009), 0812.1590.

[52] R.H. Swendsen and J.S. Wang Phys. Rev. Lett. 57, 2607 (1986).

[53] N. Metropolis, A. Rosenbluth, M. Rosenbluth, A. Teller, and E. Teller, Journal of Chemical Physics **21**, 1087 (1953).

[54] W. Hastings, Biometrika **97**, 57 (1970).

[55] N. J. Cornish and J. Crowder, Phys. Rev. D **72** (2005).

[56] T. B. Littenberg and N. J. Cornish, Phys. Rev. D **82**, 103007 (2010) [arXiv:1008.1577 [gr-qc]].

[57] T. Bogdanovic, C. S. Reynolds and M. C. Miller, arXiv:astro-ph/0703054.

[58] R. N. Lang, S. A. Hughes and N. J. Cornish, arXiv:1101.3591 [gr-qc].

[59] F. D. Ryan, "Gravitational waves from the inspiral of a compact object into a massive, axisymmetric body with arbitrary multipole moments," Phys. Rev. D **52**, 5707 (1995).

[60] N. A. Collins and S. A. Hughes, "Towards a formalism for mapping the spacetimes of massive compact objects: Bumpy black holes and their orbits," Phys. Rev. D **69**, 124022 (2004)

[61] E. Berti, V. Cardoso and C. M. Will, "On gravitational-wave spectroscopy of massive black holes with the space interferometer LISA," Phys. Rev. D **73**, 064030 (2006)

[62] E. Berti, J. Cardoso, V. Cardoso and M. Cavaglia, "Matched-filtering and parameter estimation of ringdown waveforms," Phys. Rev. D **76**, 104044 (2007)

[63] S. A. Hughes, "(Sort of) Testing relativity with extreme mass ratio inspirals," AIP Conf. Proc. **873**, 233 (2006)

[64] K. G. Arun, B. R. Iyer, M. S. S. Qusailah and B. S. Sathyaprakash, "Testing post-Newtonian theory with gravitational wave observations," Class. Quant. Grav. **23**, L37 (2006)

[65] K. G. Arun, B. R. Iyer, M. S. S. Qusailah and B. S. Sathyaprakash, "Probing the non-linear structure of general relativity with black hole mergers," Phys. Rev. D **74**, 024006 (2006)